Journal of Theoretical and Applied Mechanics, Sofia, Vol.XX (20XX) pp. 1-19
FLUID MECHANICS

FLOW AND STABILITY OF THREE-DIMENSIONAL ROTATING VISCOELASTIC JET

DANIEL N. RIAHI[1,2*]

[1]*Department of Mechanical Science and Engineering, University of Illinois at Urbana-Champaign, Urbana, IL 61801, USA*
[2]*School of Mathematical & Statistical Sciences, University of Texas Rio Grande Valley, Brownsville, Texas 78520, USA*

[Received: 27 February 2022

ABSTRACT: We consider rotationally driven nonlinear viscoelastic jet. In contrast to previous unrealistic planar studies with no gravity effect, we investigate here realistic three-dimensional jet with gravity effect. Using theoretical and computational methods, we develop models for such jet and its stability and determine the solutions. We find three-dimensional jet with gravity effect leads to faster and thinner jet. For jet arc length higher than its exit diameter, our calculation with typical parameter values shows that jet radius is smaller by a factor of more than 1.4 and jet speed is higher by factor of more than 2 as are compared to the exact planar jet counterpart results. Our linear stability of such jet uncovers new instability of the most critical three-dimensional spatiotemporal disturbance that grows in time very close to the three-dimensional jet exit but decays in space and can become stable for sufficiently far away from jet exit.

KEY WORDS: viscoelastic jet; rotating jet; gravity force; three-dimensional jet; jet stability.

1 INTRODUCTION

In the last two decades there have been a number of studies of the dynamics of the rotationally driven jet flows [1–15] for either inviscid, Newtonian viscous or non-Newtonian fluid flow cases. An essential and relevant assumption for the theoretical investigations has been the so-called slender jet theory, where as in the experimental observation and the technological applications the aspect ratio for the fiber jet is considered to be sufficiently small.

Authors in [1] carried out theoretical modeling and computation of an inviscid jet that was generated by a rotating drum. They included effects of both gravity and

*Corresponding author e-mail: d-riahi@illinois.edu

surface tension, and their investigation was based on the asymptotic and numerical techniques. For their steady solution, they calculated only the jet centerline for different values of the parameters. They found that the effect of gravity was to push down the centerline of the inviscid jet in the downward direction.

Authors in [2] studied a model for an inviscid thin liquid jet that was generated by a rotating orifice and was under a restricted two-dimensional condition that the jet centerline was in a fixed horizontal plane. The authors included effect of surface tension, but the effect of gravity was neglected. They determined, in particular, the trajectory of the jet and calculated the linear stability of the inviscid jet and found that such jet is unstable. Modeling and computation of a restricted two-dimensional inviscid rotating jet was done in [7]. The authors' modeling system was a simplified model of a centrifugal spinning system for the production of fiber jet that was developed experimentally [6] and was referred to as forcespinning process. In such a process a fluid jet is forced through an orifice of a rotating spinneret that leads to the formation of a jet with curved centerline. The authors solved numerically their inviscid modeling system, and they calculated, in particular, fiber jet radius versus arc length and for different values of the parameters that represented effects due to the rotation and surface tension. Their results indicated that jet radius was decreased with increasing the rotation rate. A model of two-dimensional steady rotating curved jet was studied in [13]. The authors carried out temporal stability of such jet and found it is unstable.

Authors in [10] used high speed photography to gain some understanding on the mechanisms involved for the production of fiber jets through the forcespinning process. They also determined the effects of some controllable parameters such as, in particular, angular velocity of the rotating spinneret and viscosity effect of the polymeric solution, which was a weight percentage of PEO (Polyethylene oxide) concentration in water, on the fiber jet speed and the jet diameter. The authors observed in their experimental fiber jet formation presence of a traveling wave disturbances, which may have been stabilized by presence fluid container, and they also acknowledged that the presence of the gravity force contributed some effects on their experimental results.

Author in [14] investigated two-dimensional rotating viscoelastic jet during forcespinning process and used the Giesekus constitutive equations [15–17] for the stress tensor in the governing equations for the jet system. He then applied scaling and perturbation techniques to determine a relatively simple system for the jet that was under restricted two-dimensional condition as in [2] and [13]. He calculated the steady solutions for the two-dimensional jet quantities and in the absence of the gravity effect. He found, in particular, that the jet speed, tensile force and stretching rate increase, while the fiber jet radius decreases, with increasing the rotation rate, the viscoelastic

effect and the arc length distance from the jet exit. Author in [15] carried out stability of two-dimensional steady solution of the rotating viscoelastic jet [14] with respect to infinitesimal two-dimensional disturbances whose wave numbers were assumed constants, and they could grow in time, space or simultaneously in time and space. He presented instability results due to the critical disturbance with constant wave number that was imposed on the two-dimensional jet. Author in [18] studied nonlinear rotating jets of viscoelastic Boger fluids during forcespinning process. The author described and used upper-convected Maxwell model for the viscoelastic aspect of the governing system of equations and the boundary conditions that were solved for the parameter regimes that were relevant to Boger fluids cases. The steady solutions for different jet quantities like stretching force, curvature and compressive force were determined.

In the present study and in contrast to the previous restricted and unrealistic two-dimensional work [14, 15], we consider realistic three-dimensional form of the nonlinear rotating viscoelastic fiber jet that includes effect of gravity force and with no restriction on the jet centerline in the three-dimensional space. Our jet system takes into account the upper-convected Maxwell model that was used before [18] in the author's modeling of nonlinear viscoelastic jet during electospinning. We first determine steady solutions of the jet quantities versus arc length and for different values of the parameters. In contrast to the planar case [14], we find that the three dimensionality of the jet system and presence of gravity force amplify resultant force that drive the jet leading to thinner and higher jet speed as well as enhancing the tensile force and more so with increasing the arc length, rotational forces and relaxation time.

As were given both briefly in the abstract part and with more details in paragraphs in Sections 3 and 5, our find that the values of three-dimensional jet quantities such as jet radius and speed that are lower and higher, respectively, as compare to the same planar jet counterpart cases. This is a consequence of the more complete three-dimensional jet system that includes, in particular, more complete forms of viscoelasticity, rotational and gravity forces, which implied modeling three-dimensional jet system in more efficient for using in applications and in predicting experimental predictions of the results.

Next, we study linear stability of such jet with respect to both two- and three-dimensional travelling wave disturbances that may grow in time, space, or simultaneously in time and space. In contrast to the restricted planar steady flow and planar disturbances with constant wave numbers [15], we detect presence of the most critical disturbances to be in three-dimension with jet arc length dependence of their wave numbers. The instabilities due to such temporal or spatial disturbances decay to zero in time or space, respectively. However, new three-dimensional spatiotemporal instability due to some critical disturbance is discovered that grows in time for region very

close to the three-dimensional jet exit but decays in space and can become negligibly small and decays to zero for sufficiently far distance from the jet exit section in a time interval that can allow for the linear stability analysis to be valid. Such instability is distinct in the sense that its growth rate, wave number and wave speed are dependent on the three-dimensional jet centerline arc length, and these quantities increase wit the arc length.

2 Governing Modeling System

Our present modeling is initially based on the original three-dimensional governing equations for the momentum and mass conservation [19] in a rotating coordinate system that is attached and embedded on a rotating spinneret (Fig. 1) for a rotating system such as that of the force-spinning [7, 10]. As in the force-spinning process, the produced fibers are curved due to the rotational forces (centrifugal and Coriolis forces).

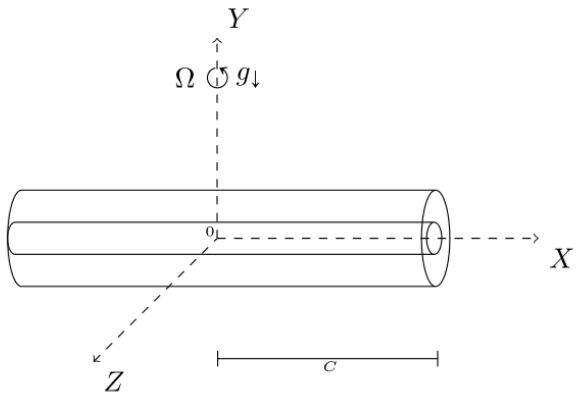

Fig. 1: Rotating spinneret and coordinate system.

The governing equations for mass continuity and momentum for the viscoelastic jets in the rotating frame, where here the stress tensor $\mathbf{T}$ is based on the upper-convected Maxwell [18, 19], are given below:

$$\nabla \cdot \mathbf{u} = 0\,, \tag{1a}$$

$$\frac{\partial \mathbf{u}}{\partial t} + \mathbf{u}\cdot\nabla\mathbf{u} = -\frac{1}{\rho}\nabla P + \frac{1}{\rho}\nabla\cdot\mathbf{T} - \omega\times(\omega\times\mathbf{r}) - 2\omega\times\mathbf{u} + \mathbf{g}\,, \tag{1b}$$

$$\mathbf{T} = \boldsymbol{\tau} + \eta_s(\nabla\mathbf{u} + \nabla\mathbf{u}^T)\,, \tag{1c}$$

$$\lambda\frac{\partial \boldsymbol{\tau}}{\partial t} + \boldsymbol{\tau} + \lambda(\mathbf{u}\cdot\nabla\boldsymbol{\tau} - \nabla\mathbf{u}^T\cdot\boldsymbol{\tau} - \boldsymbol{\tau}\cdot\nabla\mathbf{u}) = \eta_p(\nabla\mathbf{u}^T + \nabla\mathbf{u})\,, \tag{1d}$$

where $\mathbf{u}$ is the relative velocity vector of the fiber jet, P is the pressure, $\mathbf{T}$ is the stress tensor, ρ is the density of the melt or solution, $\mathbf{g}$ is the force of gravity per unit mass, t is the time variable, ω is the angular velocity vector with magnitude Ω of the rotating spinneret whose orifice emits fiber jet from the melt or solution in the fluid container [7, 10], $\mathbf{r}$ is a position vector of a point on the fiber, η_p and η_s are the viscosities of the polymer and solvent, respectively and λ is the relaxation time. We consider a Cartesian coordinate system (X, Y, Z) which is attached to the rotating spinneret (Fig. 1). This coordinate system is fixed relative to the rotating spinneret. In contrast to the previous two-dimensional studies [2, 14], where the jet centerline was restricted to be a fixed horizontal plane and gravity effect was totally neglected, we consider a three-dimensional model, where there is no such restriction, and also includes the force of gravity, and the fiber jet's arc length condition that needs to be satisfied here is given below:

$$\left(\frac{\partial \mathbf{X}}{\partial s}\right)^2 + \left(\frac{\partial \mathbf{Y}}{\partial s}\right)^2 + \left(\frac{\partial \mathbf{Z}}{\partial s}\right)^2 = 1\,, \tag{1e}$$

where s is the arc length along the jet's centerline. Thus, it is designated that the components of a position vector of a point on the jet's centerline with respect to the rotating Cartesian coordinate (X, Y, Z) system are $\mathbf{X}$, $\mathbf{Y}$ and $\mathbf{Z}$, respectively.

The governing equations (1a)–(1e) are subjected to the relevant boundary conditions for the jet. At the free surface of the jet, the kinematic and dynamic boundary conditions [19] are

$$\frac{\partial \beta}{\partial t} + \mathbf{u}\cdot\nabla\beta = 0\,, \quad \beta \equiv n - R(s,\varphi,t)\,, \tag{1f}$$

$$(\mathbf{T} - P\mathbf{I})\cdot\mathbf{n} = -\sigma\kappa\mathbf{n}\,, \tag{1g}$$

where n and φ are the radial variable and the azimuthal angle, respectively, representing the variables of the polar coordinate in a plane perpendicular to the centerline of the jet, $\mathbf{n}$ is a unit normal vector perpendicular to the jet's surface boundary pointing out of the jet, $\mathbf{I}$ is a unitary matrix, R is the radius of the jet, σ is surface tension, and $\kappa \equiv \nabla\cdot\mathbf{n}$ is twice mean curvature of the jet boundary. Similar to the earlier treatment [2, 14, 18], we presented these boundary conditions (1f)–(1g) in terms of independent variables of a local orthogonal curvilinear coordinates (s, n, φ). In addition, the following main boundary conditions at the orifice where jet exits need to be satisfied

$$\mathbf{X} = \mathbf{Y} = \mathbf{Z} = \frac{\partial \mathbf{Y}}{\partial s} = \frac{\partial \mathbf{Z}}{\partial s} = 0\,, \quad \frac{\partial \mathbf{X}}{\partial s} = 1\,, \quad u = U\,, \quad R = r_{\rm o} \text{ at } s = 0\,, \tag{1h}$$

where U is the centerline velocity of the jet at the exit section and $r_{\rm o}$ is the radius of the orifice at the jet exit section.

We non-dimensionalize the governing system (1a)–(1h) in the orthogonal coordinate system (s, n, φ) that was described before by using scaling U for velocity vector $\mathbf{u} = (u, v, w)$, ρU^2 for pressure, r_o for n and R, C for s and (X, Y, Z), C/U for t and $(\eta_s + \eta_p)U/r_0$ for the stress tensor, where C is half of length of the spinneret. For simplicity of notation we express the resulting non-dimensional variables in the governing system in terms of the same original symbols. The non-dimensional form of the stated system will contain non-dimensional parameters Rossby number $\mathrm{Rb} = U/(\Omega C)$ representing the rotational parameter, Froude number $\mathrm{F} = U/(Cg)^{0.5}$ representing the gravity parameter, Weber number $\mathrm{We} = \rho U^2 r_o/\sigma$ representing the surface tension parameter, Reynolds number $\mathrm{Re} = \rho UC/(\eta_s + \eta_p)$ representing the viscosity parameter, Deborah number $\mathrm{De} = \lambda U/C$ representing the viscoelastic parameter, viscosity ratio $\eta = \eta_p/(\eta_s + \eta_p)$ for the polymer and solvent viscosities and a small aspect ratio parameter $\varepsilon = r_o/C$ ($\varepsilon \ll 1$), where g is acceleration due to gravity and λ is the relaxation time.

Similar to the previous studies [2, 14, 18], the present dimensionless system that contains ε, is under the relevant assumption that the fiber jet is a long and slender object, so that ε is considered a very small parameter ($\varepsilon \ll 1$) for an scaling analysis that we consider with the following related expansions for the dependent variables:

$$
\begin{aligned}
&\text{(2a)} \quad (u, v, w) = [u_0(s,t) + \varepsilon n u_1(s\varphi, t) + \cdots, \varepsilon n v_1(s, \varphi, t) + \cdots, \\
&\qquad\qquad \varepsilon n w_1(s, \varphi, t) + \cdots], \\
&\text{(2b)} \quad (P, R) = [P_0(st) + \varepsilon n P_1(s, \varphi, t) + \cdots, R_0(s,t) + \varepsilon R_1(s, \varphi, t) + \cdots], \\
&\text{(2c)} \quad (X, Y, Z) = [X_0(s,t) + \varepsilon X_1(s,t) + \cdots, Y_0(s,t) + \varepsilon Y_1(s,t) + \cdots, \\
&\qquad\qquad Z_0(s,t) + \varepsilon Z_1(s,t) + \cdots], \\
&\text{(2d)} \quad \tau_{ij} = \tau_{0ij}(s)\delta_{ij} + \varepsilon n \tau_{1ij}(s, \varphi) + \cdots,
\end{aligned}
$$

where subscripts "ij" for τ_{ij} in (2d) indicate that normal stress components along s and n directions, respectively, are for $i = j = 1$ and 2, while tangential components of the stress tensor correspond to the case where $i \neq j$. Also δ_{ij} defined to be equal 1 if $i = j$ and 0 if $i \neq j$.

Our scaling analysis then makes use of the above expansions in the governing system, where the scaling factor ε is used to scale the variables properly in the governing system. The governing systems are then simplified and only the leading order terms in (1a)–(1e) are retained and further simplifications are made to have a final system only for u_0, R_0, X_0, Y_0 and Z_0. Dropping the subscripts for simplicity of notations, the resulting simplified form of the modeling system is given below:

$$\text{(3a)}\quad \frac{\partial u}{\partial t}+u\Big[E_8\frac{\partial}{\partial t}\frac{\partial X}{\partial s}+E_9\frac{\partial}{\partial t}\frac{\partial Y}{\partial s}+E_{10}\frac{\partial}{\partial t}\frac{\partial Z}{\partial s}\Big]+u\frac{\partial u}{\partial s}$$
$$=\frac{1}{\mathrm{We}\,R^2}\frac{\partial R}{\partial s}-\frac{E_9}{\mathrm{F}^2}+\frac{2u}{\mathrm{Rb}}\Big[E_8\frac{\partial Z}{\partial s}-E_{10}\frac{\partial X}{\partial s}\Big]+\frac{1}{\mathrm{Rb}^2}[E_8(X+1)+E_{10}Z]$$
$$+\frac{1-\eta}{\mathrm{Re}}\Big[\frac{6}{R}\frac{\partial R}{\partial s}\frac{\partial u}{\partial s}+2\frac{\partial^2 u}{\partial s^2}\Big]+\frac{1}{\mathrm{Re}\,R^2}\frac{\partial}{\partial s}[R^2(\tau_{11}-\tau_{22})],$$

$$\text{(3b)}\quad \frac{\partial R}{\partial t}+u\frac{\partial R}{\partial s}=-\frac{R}{2}\frac{\partial u}{\partial s}\,,$$

$$\text{(3c)}\quad E_0u\frac{\partial}{\partial s}\Big\{\frac{1}{E_0}\Big[\frac{\partial X}{\partial s}\frac{\partial^3 X}{\partial s^3}+\frac{\partial Y}{\partial s}\frac{\partial^3 Y}{\partial s^3}+\frac{\partial Z}{\partial s}\frac{\partial^3 Z}{\partial s^3}\Big]\Big\}$$
$$=\frac{3}{2}\frac{\partial u}{\partial s}\Big[\frac{\partial X}{\partial s}\frac{\partial^3 X}{\partial s^3}+\frac{\partial Y}{\partial s}\frac{\partial^3 Y}{\partial s^3}+\frac{\partial Z}{\partial s}\frac{\partial^3 Z}{\partial s^3}\Big],$$

$$\text{(3d)}$$
$$-u\Big[E_{11}\frac{\partial}{\partial t}\frac{\partial X}{\partial s}-E_{12}\frac{\partial}{\partial t}\frac{\partial Y}{\partial s}+E_{13}\frac{\partial}{\partial t}\frac{\partial Z}{\partial s}\Big]+\Big[-u^2+\frac{1}{\mathrm{We}\,R}\Big]E_0$$
$$-\frac{u}{\mathrm{Rb}}\Big[E_{11}\frac{\partial Z}{\partial s}-E_{13}\frac{\partial X}{\partial s}\Big]+\frac{E_12}{\mathrm{F}^2}+\frac{1}{\mathrm{Rb}^2}[E_{11}(X+1)-E_{13}Z]$$
$$+\frac{1}{\mathrm{Re}}\Big[2\frac{\partial}{\partial s}(uE_0)+\frac{E_0}{6}\frac{\partial u}{\partial s}-\frac{u}{3}\frac{\partial E_0}{\partial s}\Big]=0,$$

$$\text{(3e)}\quad \Big(\frac{\partial X}{\partial s}\Big)^2+\Big(\frac{\partial Y}{\partial s}\Big)^2+\Big(\frac{\partial Z}{\partial s}\Big)^2=1\,,$$

$$\text{(3f)}\quad \tau_{11}+\mathrm{De}\Big[\frac{\partial \tau_{11}}{\partial t}+u\frac{\partial \tau_{11}}{\partial s}-2\tau_{11}\frac{\partial u}{\partial s}+\frac{\mu}{\eta}\tau_{11}^2\Big]=2\eta\frac{\partial u}{\partial s}\,,$$

$$\text{(3g)}\quad \tau_{22}+\mathrm{De}\Big[\frac{\partial \tau_{22}}{\partial t}+u\frac{\partial \tau_{22}}{\partial s}+\tau_{22}\frac{\partial u}{\partial s}+\frac{\mu}{\eta}\tau_{22}^2\Big]=-\eta\frac{\partial u}{\partial s}\,,$$

where the expressions for E_0 – E_{13} are of the form given in [18] and are not given here.

The boundary conditions are given by

$$\text{(4a)}\quad X=Y=Z=\frac{\partial Y}{\partial s}=\frac{\partial Z}{\partial s}=u-1=R-1=\frac{\partial X}{\partial s}-1=0\ \text{ at }\ s=0$$

$$\text{(4b)}\quad \tau_{11}-2\eta\frac{\partial u}{\partial s}=\tau_{22}+\eta\frac{\partial u}{\partial s}=0\ \text{ at }\ s=0\,,$$

where the stress conditions in (4b) are of the form as given in [18].

3 Steady Solutions and Results

The asymptotic form of the steady solution for small s and the corresponding results for the dependent variables, which were found to be useful as initial conditions for

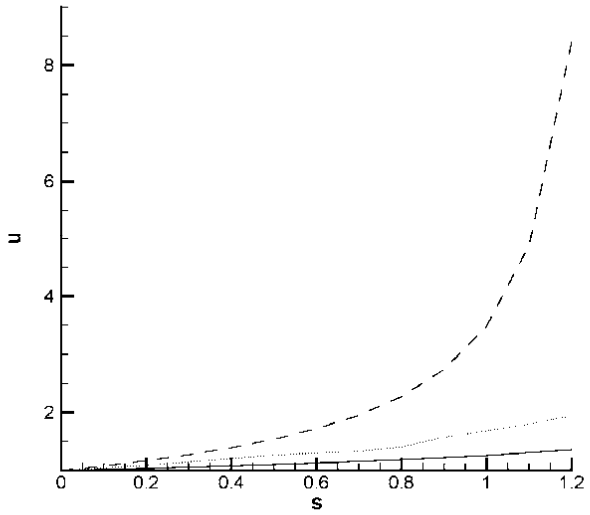

Fig. 2: Jet speed versus arc length for We $= 1.5$, Re $= 1.0$, De $= 1.0$, $\eta = 0.1$, F $= 4.0$ and three different values of Rossby number Rb $= 1$ (dashed line), 1.3 (dotted line) and 2.0 (solid line).

our numerical solutions of (3a)–(3g) and (4a)–(4b), are not given here but can be found with further details in [18]. We solved the nonlinear steady system (3a)–(3g) and (4a)–(4b) numerically by treating it as an initial value problem with independent variable s using an efficient Runge-Kutta scheme of fourth order [21]. We obtained the numerical solution for the described initial value problem, and we generated data for the jet quantities with different values of the parameters.

Figure 2 presents jet speed versus arc length for We $= 1.5$, Re $= 1.0$, F $= 4.0$, De $= 1.0$, $\eta = 0.1$ and different values of the Rossby number. It can be seen from this figure that the effect of rotational forces enhancing the jet in the sense that the jet speed increases with the rotation rate. and more rapidly with increasing the arc length. Our additional generated data for higher values of the Deborah number indicated similar enhancing effect of the rotational forces. As compared with the corresponding results in the restricted two-dimensional case [14], the rate of increase of jet speed with respect to the rotation rate and the arc length in the present three-dimensional system was found to be notably higher than in the two-dimensional case.

Figure 3 is the same as Fig. 2 but for tensile force [$T_f = R^2\,(\tau_{11} - \tau_{22})$] [20] versus arc length. It can be seen from this figure that the tensile force increases significantly with increasing the rotation rate and its arc length rate of change enhance notably with increasing the arc length for the value of the rotation rate beyond some

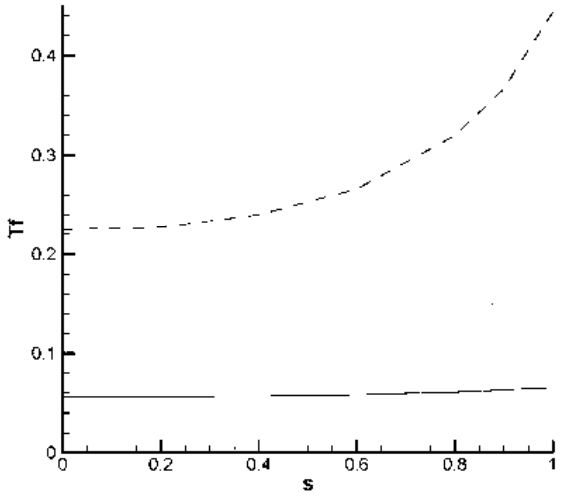

Fig. 3: The same as in Fig. 2 but for tensile force versus arc length.

value. Our additional generated data for the tensile force versus arc length for given values of Rb, Re, We, η and De but for different values of F indicated evidence for the enhancing effect due to gravity on the tensile force, which increases more with the arc length and the gravity effect. This also indicates importance effect of three-dimensionality of the jet with the presence of the gravity that need to be accounted for.

Figure 4 presents jet radius versus arc length for Rb $=$ 2.0, Re $=$ 1.0, F $=$ 4, We $=$ 1.5, η $=$ 0.1 and 2 different values of the Deborah number. It can be seen from figure 4 that jet radius decreases with increasing the arc length and the viscoelastic effect, which indicates similar roles played by the relaxation time of the non-Newtonian fluid flow. It also shows that the jet radius decreases with increasing both the viscoelasticity and the arc length especially if the jet is not too close to its exit section.

Our results also indicated that the jet radius in the present three-dimensional model is notably smaller as compare with those for the two-dimensional viscoelastic jet and the Newtonian jet cases [7, 14]. Thus, three-dimensionality of the jet system as well as presence of gravity force and the non-Newtonian viscoelastic nature of the fiber jet are all enhancing the jet formation notably in the present jet flow.

For a more direct comparison of the results of the present three-dimensional jet system and the counterpart for the planar jet system, we carried out calculations of the jet quantities in the two systems for Re $=$ 1.0, We $=$ 1.3, Db $=$ 1.0, Rb $=$ 2.0,

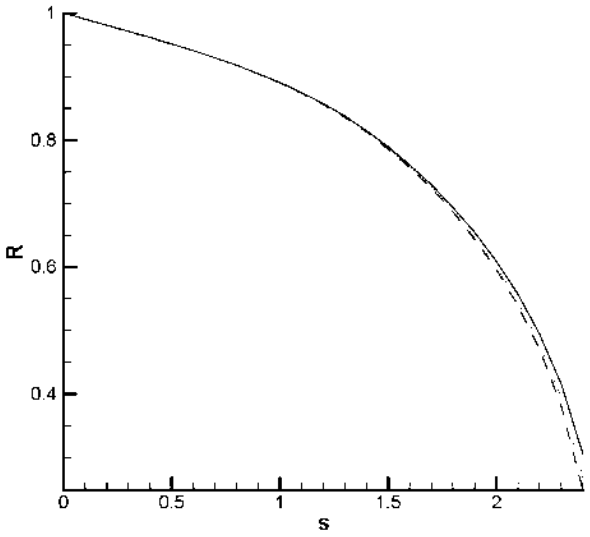

Fig. 4: Jet radius versus s for Re $= 1.0$, Rb $= 2.0$, F $= 4.0$, We $= 1.5$, $\eta = 0.1$ and different cases of De $= 15.0$ (dashed line) and 1.0 (solid line).

F $=$ (4.0 for three-dimensional case; ∞ for planar case) and $\eta = 0.1$. Table 1 below provides results for discrete values of jet radius and speed versus arc length for both systems.

It can be seen from Table 1 that jet for three-dimensional case begins to become notably thinner than its two-dimensional analog for $s \geq 2.0$ while jet speed for three-dimensional case starts to become notably bigger that its two-dimensional analog for $s \geq 2.0$. These parameter values that were chosen in table 1 are considered typical for the reasons thay are given as follow. Our additional calculations for different parameter values indicated similar qualitative results. In addition our our further

Table 1: Values of jet radius and speed for different values of the arc length for both three-dimensional jet (F $= 4.0$) and its two-dimensional analog (F $= \infty$) with Re $= 1$, We $= 1.3$, Db $= 1.0$, Rb $= 2.0$ and $\eta = 0.1$

s	0.0	0.4	0.8	1.2	1.6	1.8	2.0	2.2	2.4
3D radius	1.000	0.962	0.918	0.858	0.761	0.694	0.609	0.494	0.306
2D radius	1.000	0.963	0.929	0.899	0.879	0.873	0.870	0.868	0.866
3D speed	1.000	1.082	1.187	1.359	1.725	2.075	2.694	4.097	10.676
2D speed	1.000	1.079	1.160	1.236	1.295	1.313	1.321	1.324	1.328

studies of other jet quantities indicated that similar qualitative results with jet speed were found for other jet quantities such as tensile force, stretching force and strain rate. Thus, such results indicated that three-dimensionality of jet in the presence of gravity force enhance the effectiveness of the jet, which is more in agreement with experimental results [10] for the jet fiber and effectiveness of forcespinning process to produce fiber.

We also find from the results given in table 1 that rate of increase and decrease of three-dimensional jet speed and jet radius, respectively, with respect to arc length increase and decrease with increasing the arc length and are significantly higher than for the two-dimensional jet speed and radius counterpart. Our additional calculations indicated that similar to the above results for three-dimensional jet speed and jet radius their rate of increase and decrease, respectively, with respect to viscoelasticity, rotational forces or gravity force are notably higher than for the two-dimensional jet quantities counterpart.

4 Linear Stability Analysis and Results

We consider dependent variables for the three-dimensional jet flow that satisfy the system (3a)–(3g) and (4a)–(4b) to be sum of dependent variables for the steady jet flow solutions plus three-dimensional corresponding dependent variables for sufficiently small amplitude of time-dependent disturbances in the form of travelling waves as were observed experimentally [10]. Thus, for the linear stability investigation of the steady state of the jet, we superimpose the three-dimensional disturbance flow on the three-dimensional steady flow. In general, such disturbances can grow or decay exponentially in time alone, grow or decay in space alone or simultaneously grow or decay in both time and space.

Following [2] and the slender jet theory, where the ratio of the length scale of the jet centerline to that for the jet radius is of order ε ($\varepsilon \ll 1$), we take into account presence of three-dimensional flow of small-amplitude disturbances that is superimposed on the three-dimensional steady jet flow. We consider such disturbances in the form of travelling waves whose dependent variables have the following expressions:

$$(5)\quad (u', R', X', Y', Z', \tau_{11}', \tau_{22}') = [\varepsilon u^*(s), R^*(s), \varepsilon^3 X^*(s), \varepsilon^3 Y^*(s), \varepsilon^3 Z^*(s), \tau_1^*(s), \tau_2^*(s)]T,$$
$$T \equiv \exp[k(s)s_1 + \lambda(s)t_1]\,.$$

Here $s_1 = s/\varepsilon, t_1 = t/\varepsilon, k(s) = O(1)$ is complex growth rate in space, $\lambda(s) = O(1)$ is complex growth rate in time and quantities with superscript star are the s-dependent coefficients of the disturbance variables. We, thus, use a multi-scale formulation of

the type used before [2] and take into account disturbances with wavelengths of order ε as needed.

We should note from (5) that we included ε and ε^3 factors in the expressions for the disturbance quantities u^*, X^*, Y^* and Z^* as we found to be needed. Because if we omit these factors, then it was found that the leading order disturbances for these variables were identically zero and the first non-zero leading order disturbances are those as given in (5). Also as in [2, 15], we require that the product of the disturbance frequency and wave number to be negative in order for the travelling disturbance waves to propagate away from the jet exit section.

We consider the dependent variables in the equations (3a)–(3g) to be as sum of the corresponding dependent variables for the steady flow and the disturbances. We use these in the equations (3a)–(3g), subtract the equations for the steady flow from the corresponding ones in these equations and linearize the resulting system with respect to the amplitude of the disturbances. We then obtain the following system of equations to the leading order terms in ε that we shall use for the linear stability analysis of the steady flow:

$$\text{(6a)}\quad \frac{\partial u'}{\partial t_1}+u\frac{\partial u'}{\partial s_1}=\frac{1}{\mathrm{We}}\frac{\partial R'}{\partial s_1}+\frac{1-\eta}{\mathrm{Re}}\Big[6R\frac{du}{ds}\frac{\partial R'}{\partial s_1}-R^2\frac{\partial^2 R'}{\partial s_1^2}\Big] + \frac{1}{\mathrm{Re}}\Big\{2R(\tau_{11}-\tau_{22})\frac{\partial R'}{\partial s_1}+R^2\Big[\frac{\partial \tau_1'}{\partial s_1}-\frac{\partial \tau_2'}{\partial s_1}\Big]\Big\},$$

$$\text{(6b)}\quad \frac{\partial R'}{\partial t_1}+u'\frac{\partial R}{\partial s}+u\frac{\partial R'}{\partial s_1}+\frac{1}{2}\Big[R'\frac{\partial u}{\partial s}+R\frac{\partial u'}{\partial s_1}\Big]=0\,,$$

$$\text{(6c)}\quad \frac{\partial X}{\partial s}\frac{\partial X'}{\partial s_1}+\frac{\partial Y}{\partial s}\frac{\partial Y'}{\partial s_1}+\frac{\partial Z}{\partial s}\frac{\partial Z'}{\partial s_1}=0\,,$$

$$\text{(6d)}\quad -5u\frac{\partial}{\partial s_1}\Big[\frac{dX}{ds}\frac{\partial^3 X'}{\partial s_1^3}+\frac{dY}{ds}\frac{\partial^3 Y'}{\partial s_1^3}+\frac{dZ}{ds}\frac{\partial^3 Z'}{\partial s_1^3}\Big]+6.5E_0^2\frac{\partial u'}{\partial s_1}=0\,,$$

$$\text{(6e)}\quad u\Big[\frac{dX}{ds}\frac{\partial^4 X'}{\partial s_1^4}+\frac{dY}{ds}\frac{\partial^4 Y'}{\partial s_1^4}+\frac{dZ}{ds}\frac{\partial^4 Z'}{\partial s_1^4}\Big] = \frac{3}{2}\frac{du}{ds}\Big[\frac{dX}{ds}\frac{\partial^3 X'}{\partial s_1^3}+\frac{dY}{ds}\frac{\partial^3 Y'}{\partial s_1^3}+\frac{dZ}{ds}\frac{\partial^3 Z'}{\partial s^3}\Big] + \frac{3}{2}\Big[\frac{dX}{ds}\frac{d^3 X}{ds^3}+\frac{dY}{ds}\frac{d^3 Y}{ds^3}+\frac{dZ}{ds}\frac{d^3 Z}{ds^3}\Big]\frac{\partial u'}{\partial s_1}\,,$$

$$\text{(6f)}\quad \tau_2'+\mathrm{De}\Big[\frac{\partial \tau_2'}{\partial t_1}+\frac{\partial}{\partial s_1}(u\tau_2'+u'\tau_{22})\Big]+\frac{2\mu\mathrm{De}}{\eta}(\tau_2'\tau_{22})+\eta\frac{\partial u'}{\partial s_1}=0\,,$$

$$\text{(6g)}\quad \tau_1'+\mathrm{De}\Big\{-2\Big[\tau_1'\frac{du}{ds}+\tau_{11}\frac{\partial u'}{\partial s_1}\Big]+u\frac{\partial \tau_1'}{\partial s_1}+\frac{\partial \tau_1'}{\partial t_1}\Big\}+2\frac{\mu\mathrm{De}}{\eta}(\tau_1'\tau_{11})-2\eta\frac{\partial u'}{\partial s_1}=0\,.$$

Using (5) in (6a)–(6g) for the disturbance quantities and dividing each equation by T, we find seven linear algebraic equations for the s-dependent coefficients u^*, R^*, X^*, Y^*, Z^*, τ_1^* and τ_2^* of the disturbance quantities. It is found necessary to assume that all these s-dependent coefficients for the dependent variables of the disturbances are non-zero otherwise no non-zero disturbances are found to be counted.

For the temporal instability case, we have $\lambda = \lambda_r + i\lambda_i$ and $k = ik_i$, where λ_r is the real growth rate, $i = (-1)^{0.5}$ is pure imaginary number, λ_i is the frequency of the travelling wave disturbance and k_i is the centerline wave number. The leading order terms in ε [O(1/ε)] in the resulting equations from (6b), (6f) and (6g) then lead to $\lambda + ik_iu = 0$, which implies that $\lambda_r = 0$ and $\lambda_i/k_i = -u$. Thus, no temporal instability is possible, and the disturbances are simply travelling waves with zero growth rates, and the speed of such waves increases with distance along the jet. These waves also propagate away from the jet exit section since $u > 0$ as we found earlier in Section 3 and so $\lambda_i/k_i < 0$.

For the spatial stability case, we have $\lambda = i\lambda_i$ and $k = k_r + ik_i$, where the growth rate of the disturbance is k_r. The leading order terms in ε in the resulting equations from (6b), (6f) and (6g) then lead to $uk + i\lambda_i = 0$, which implies that $k_r = 0$ and $\lambda_i/k_i = -u$. Thus, no spatial instability is possible, and the disturbances are again travelling waves with zero growth rates in both time and space. Similar to the temporal stability case, these waves propagate away from the jet exit section, and their speed increases with the arc length distance along the jet.

Next we consider linear stability of the steady flow with respect to disturbances that can simultaneously grow or decay in both time and space. Thus, we set $\lambda = \lambda_r + i\lambda_i$ and $k = k_r + ik_i$ that both can be complex in general. Using these in (6a)–(6g), we find that the leading order terms in (6b), (6f) and (6g) then lead to $\lambda + ku = 0$, which implies that $\lambda_r = -k_ru$ and $\lambda_i/k_i = -u$. It can be seen from these results that disturbance wave propagates away from the jet exit and its speed increases with arc distance along the jet. The temporal growth rate is positive if the special growth rate is negative, and vice versa spatial growth rate is positive if temporal growth rate is negative.

To determine more information about the growth rate for such disturbances, we find that the leading order terms in the simplified form of the equations (6c)–(6e) are in terms of unknown k, X^*, Y^*, Z^* and u^*, which are non-zero as we explained before. In addition, these three equations contain some of the dependent variables of the steady solution that are considered to be given quantities for given values of the parameters. From these equations, we find X^*, Y^* and Z^* in terms of ku^*. Next, we use the simplified form of equations (6b) and (6f)–(6g) to find ku^*, τ_1^* and τ_2^* in terms of kR^* and some of the known quantities for the dependent variables of the steady flow. We then use these in the simplified form of (6a) to find a linear algebraic

equation for (dk/ds) whose coefficients are very lengthy functions of the arc length and the jet parameters and will not be given here. Considering non-zero k and non-zero (dk/ds), we calculate the solutions to this algebraic equation by iteration for given values of the parameters that can correspond to particular steady flow solutions. We find that both k_i and k_r are dependent on the jet arc length, and we calculate k_r and k_i for different values of the parameters and s. We found that regardless of the values of the parameters, k_r remains negative and k_i is positive, and the magnitudes of both of these quantities appear to increase with the arc length. Thus, going back to the relation $\lambda_r = -uk_r$, we see that the temporal growth rate of the spatiotemporal instability is positive, while clearly from this relation the spatial growth rate of the spatiotemporal instability is negative.

Figures 5 and 6 present, respectively, some typical values for temporal growth rate and centerline wave number of the spatiotemporal disturbances that can cause instability versus arc length for F $= 4.0$, We $= 1.5$, Re $= 1.0$, $\eta = 0.1$ and different values of Rb and De. The results that are given below are based on these figures as well as from our additional calculations for different values of the parameters that we determine the temporal growth rate and the wave number of the three-dimensional spatiotemporal disturbances that cause instability of the already described three-dimensional steady flow. From these Figs. 5 and 6, it can be seen

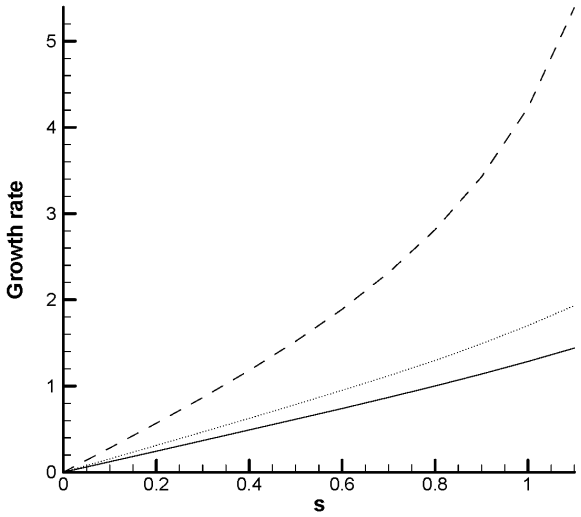

Fig. 5: Temporal growth rate of spatiotemporal instability versus s for F =4.0, W_e =1.5, Re $= 1.0$, $\eta = 0.1$ and different values of De $= 1.0$ (Rb $= 1.0$ dashed line; Rb $= 2$ solid line) and 3.0 (Rb $= 2.0$ dotted line).

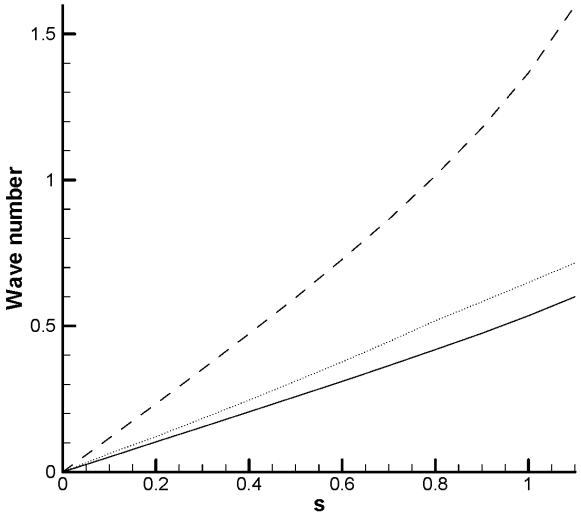

Fig. 6: The same as in Fig. 5 but for jet centerline wave number versus s.

directly that both rotational forces and viscoelasticity effects are destabilizing in the sense that they significantly increase the temporal growth rate, both of such effects reduce the wave length of the most critical growing disturbances. In addition, the wave speed of such disturbances grows with increasing the rotational forces, viscoelasticity and the jet arc length.

I can also be seen for figures 5 and 6 that the rate at which such temporal growth rate snd wave number increase with respect to the jet arc length are higher mostly for higher rotational forces and viscoelasticity. Our additional calculations indicated that such growth rate and the wave number and their rate of changes with respect to the arc length increase with the force of gravity. However, the values such growth rate and the wave number and their rates of changes with respect to the arc length decrease with increasing the surface tension and viscosity, which have stabilizing effects on the steady flow and its possible instability.

Thus, such critical disturbances superimposed on the steady solutions can increase their amplitudes in time, but their amplitudes decay in space and their wave length decreases with increasing the jet arc length. However, due to the assumed linear instability in the present analysis, such temporally unstable disturbances cannot grow indefinitely due to the assumed linear instability, and, thus, such disturbance should decay to zero for sufficiently large distance from the jet exit within a time interval where linear stability analysis is not invalidated. Our calculated results for different values of the parameters and the jet arc length indicated that the growth rates, wave

speeds and wave numbers of such disturbances can increase with the gravity effect, rotation rate and viscoelasticity but can decrease with increasing viscosity and surface tension.

5 Conclusions and Remarks

We developed models for flow and stability of three-dimensional nonlinear rotating viscoelastic jet with gravity effect. We were interested to find the effects due to the three-dimensionality of the jet, presence of the gravity force, rotational forces and the viscoelasticity on the steady solutions for the jet quantities and on the stability of such solutions. We determined the steady solutions theoretically as well as numerically. We found that in contrast to the two-dimensional results [14] the values of the jet speed and tensile force raised up considerably at higher values by the three-dimensionality of the jet and the presence of the gravity force, and these quantities of the jet increase at higher rates with increasing the arc length, rotation rate, gravity and viscoelasticity. However, the value of the jet radius dropped down notably to lower value due to the presence of the gravity and the three-dimensionality nature of the present jet system, and the jet radius decreases at higher rates with increasing the effects due to the rotation, gravity and the viscoelasticity.

We also used multiple scale technique to investigate the linear stability of the three-dimensional steady solutions versus superimposed small amplitude traveling wave disturbances in both two- and three-dimensional cases. For the most critical disturbances in time alone or in space alone, which were three-dimensional in nature, we found that the viscoelastic jet remains stable. For the most critical disturbances that can grow simultaneously in time and space and were three-dimensional, we found that linear instability is possible only within a time interval where linear stability analysis is valid, but it is required that such disturbance be in three-dimensional space and its growth rate, wave speed and wave number be dependent on the arc length of the jet.

About the comparison of the present three-dimensional results and those given in [2, 7, 13–15], for two-dimensional models that were described before in section 1, together with table 1 and the two last paragraphs that were given in Section 3, it should be emphasized that there are significant differences between the type of jet system and the results in the present work and those in above references. In the present study we provided new results about presence of three-dimensionality of the jet system and the gravity force on the three-dimensional steady solutions and the stability of such three-dimensional solutions with respect to the most critical disturbances thst were found to be three-dimensional and not two-dimensional, while the previous studies were either for inviscid jet cases [2, 7] or for viscoelastic jet cases but all such models in above references were for unrealistic two-dimensional

jet, where the jet centerline was restricted to lie in a fixed horizontal plane, and no gravity effect was included. The values of the jet speed, strain rate, tensile force and stretching rate in the present case were notably higher and more realistic in agreement with experimental evidence [10] than in any of those given in planar case, and their rate of increase with respect to the rotation rate, viscoelasticity and the arc length were significantly higher in the present case than in those for planar jet models. The jet radius was notably smaller and more realistic in the present case than that in the planar case in agreement with experiments [10], and its rates of decrease with respect to the rotation rate, viscoelasticity and the arc length were notably larger here than in the planar case. In contrast to the planar case, the curvature of jet trajectory in the present case was more correctly higher locally for higher rotation rate and the viscoelasticity and for lower surface tension and polymer viscosity.

In addition, the present three-dimensional results agree more closely with the corresponding three-dimensional experimental results [10]. About stability results, we should note that steady two-dimensional solution was temporally unstable [2, 13] or spatially unstable [2], while in the present case and in [15] steady solutions were found to be stable temporally or spatially, and only a combined three-dimensional spatiotemporal type instability was found to be possible. However, in the planar case [15] instability was detected for particular planar disturbance with restricted constant wave number whose growth rate was notably smaller than in the present most critical three-dimensional instabilities due to the particular three-dimensional disturbances whose wave numbers were found to increase with arc length. In addition, the growth rates, wave speed and wave numbers of such three-dimensional disturbances were found to increase significantly with the rotation rate, viscoelasticity, gravity and the arc length at much higher values and rates than those in the restricted planar case [15]. Thus, present realistic three-dimensional model provides significantly more new qualitative results than in the cases of planar counterpart.

In regard to the application of our investigated three-dimensional steady part for the fiber jet formation, our work is considered the first stage in the real case after the jet leaving the spinneret (Fig. 1) within the fiber production process. Thus, additional work will also be needed to investigate in future about other features of the fiber jet and ways for its variables to be controlled for ultimate fiber diameter that is strongly dependent upon the jet formation, aerodynamic ambient forces, evaporation of the solvent, humidity and temperature of the environment and collection system.

In the three-dimensional experiments carried out in [10] the authors observed traveling wave disturbances, but they did not report any instability that could have resulted from such disturbances that could have resulted in jet breakup. We also should note that the predicted very particular instability in the present study may possibly be initially formed in their experiments but then was stabilized quickly due

to the presence of other factors that were existed in the experiments such as presence of ambient flow, evaporation and solidification of the fiber jets before the fibers were collected in the container, and the container itself could also exert stabilization on the fiber jets. It is the author's desire to take into account these other factors in his future investigation.

Finally, as an applicability in the experimental studies or in the fiber production technology, it should be noted that from a modeling point of view it is important in using three-dimensional jet model in the presence of gravity to collect relevant parameter values for a given fiber jet case in order to achieve more correctly and accurately production of such fiber jet case.

ACKNOWLEDGEMENTS

The author thanks reviewers' comments and suggestions for an earlier version of this work that improved the quality of the present paper.

REFERENCES

[1] S.P. DECENT, A.C. KING, I.M. WALLWORK (2002) Free jets spun from a prilling tower. *Journal of Engineering Mathematics* **42** 265-282.

[2] I.M. WALLWORK, S.P. DECENT, A.C. KING, R.M.S.M. SCHULKES (2002) The trajectory and stability of a spiraling liquid jet: Part I. Inviscid theory. *Journal of Fluid Mechanics* **459** 43-65.

[3] E.I. PARAU, S.P. DECENT, M.J.H. SIMMONS, D.C.Y. WONG, A.C. KING (2007) Nonlinear viscous liquid jets from a rotating orifice. *Journal of Engineering Mathematics* **57** 159-179.

[4] S. PANDA, N. MARHEINEKE, R. WEGENER (2008) Systematic derivation of an asymptotic model for the dynamics of curved viscous fibers. *Mathematical Methods in Applied Sciences* **31** 1153-1173.

[5] S.P. DECENT, A.C. KING, M.J.H. SIMMONS, E.I. PARAU, I.M. WALLWORK, C.J. GURNEY, J. UDDIN (2009) The trajectory and stability of spiraling liquid jet: Viscous theory. *Applied Mathematical Modelling* **33** 4283-4302.

[6] K. SARKAR, C. GOMEZ, S. ZAMBRANO, M. RAMIREZ, E. DE HOYOS, H. VASQUEZ, K. LOZANO (2010) Electrospinning to forcespinning. *Materials Today* **13**(11) 42-44.

[7] S. PADRON, I.D. CARUNTU, K. LOZANO (2011) On 2d forcespinning modeling. In: *Proceedings of the 2011 ASME International Mechanical Engineering Congress and Exposition*, IMECE2011-64823 **7** 821-830, November 11-17, 2011, Denver, Co., USA.

[8] B. VASQUEZ, H. VASQUEZ, K. LOZANO (2012) Preparation and characterization of polyvinylidene fluoride nanofibrous membranes by forcespinning. *Polymer Engineering and Science* **52**(10) 2260-2265.

[9] A. ALTECOR, Y. MAO, K. LOZANO (2012) Large-scale synthesis of tin-doped indium oxide nanofibers using water as solvent. *Functional Materials Letters* **5**(1) 1250020.

[10] S. PADRON, A. FUENTES, K. LOZANO (2013) Experimental study of nanofiber production through forcespinning. *Journal of Applied Physics* **113**(2) 024318.

[11] S.M. TAGHAVI, R.G. LARSON (2014) Regularized thin-fiber model for nanofiber formation by centrifugal spinning. *Physical Review E* **89** 023011.

[12] S.M. TAGHAVI, R.G. LARSON (2014) Erratum: Regularized thin-fiber model for nanofiber formation by centrifugal spinning. *Physical Review E* **89** 059903(E).

[13] A.M. ALSHARIF, J. UDDIN (2015) Instability of viscoelastic curved liquid jets with surfactants. *Journal of Non-Newtonian Fluid Mechanics* **216** 1-12.

[14] D.N. RIAHI (2018) Nonlinear rotating viscoelastic jets during forcespinning process. *Proceeding of The Royal Society of London, Series A* **474** 20180346.

[15] D.N. RIAHI (2020) On stability of steady nonlinear rotating viscoelastic jets. *Applications in Engineering Science* **2** 100010.

[16] H. GIESEKUS (1982) A simple constitutive equations for polymer fluids based on the concept of configuration-dependent tensorial mobility. *Journal of Non-Newtonian Fluid Mechanics* **11** 69-109.

[17] R.B. BIRD, C.F. CURTISS, R.C. ARMSTRONG, O. HASSAGER (1987) "Dynamics of Polymeric Liquids", vol. 1, Fluid Mechanics, Wiley, New York, USA.

[18] D.N. RIAHI (2021) On forcespinning of nonlinear rotating jets of viscoelastic Boger fluids. *Journal of Non-Newtonian Fluid Mechanics* **287** 104442.

[19] R.P. CHAHHAHRA, J.F. RICHARDSON (2008) "Non-Newtonian Flow and Applied Rheology", Second Edition, Butterworth-Heinemann, Oxford, U.K.

[20] J.J. FENG (2003) Stretching of a straight electrically charged viscoelastic jet. *Journal of non-Newtonian Fluid Mechanics* **116** 55-70.

[21] U.M. ASCHER, R.M.M. MATHHEIJ, R.D. RUSSELL (1995) "Numerical Solution of Boundary Value Problems for Ordinary Differential Equations", SIAM, PA, USA.